

# Interaction of an ultra-intense laser pulse with a nonuniform preformed plasma

J. Faure, V. Malka, J.-R. Marquès, and F. Amiranoff

*Laboratoire pour l'Utilisation des Lasers Intenses, Unité Mixte de Recherche 7605 CNRS-CEA-Paris VI-Ecole Polytechnique, 91128 Palaiseau, France*

C. Courtois

*Laboratoire de Physique des Gaz et des Plasmas, Unité Mixte de Recherche 8578, CNRS, Université Paris XI, Bât 210, 91405 Orsay, France*

Z. Najmudin, K. Krushelnick, M. Salvati, and A. E. Dangor

*Imperial College, London, United Kingdom*

A. Solodov, P. Mora, J.-C. Adam, and A. Héron

*Centre de Physique Théorique, CNRS-Ecole Polytechnique, Palaiseau, France*

(Received 9 February 2000; accepted 1 March 2000)

The propagation of an ultra-intense laser pulse in a preformed plasma channel was investigated experimentally. Different regimes of propagation were observed when the pulse duration was varied. For a long pulse and powers lower than the critical power for self-focusing,  $P_L/P_C < 1$  ( $I_0 = 2 \times 10^{17}$  W/cm<sup>2</sup>), the laser pulse was guided by the preformed plasma channel over three Rayleigh lengths (4 mm) and a longitudinal plasma wave was generated by envelope self-modulation of the pulse. For a short pulse and  $P_L/P_C \gg 1$ , the interaction was dominated by self-focusing and Raman instabilities. Numerical simulations were run for the latter case, giving results comparable to the experiment. The simulations were also used to investigate the dynamics of the instabilities at high power. They showed that strong Raman side scattering first occurs at the beginning of the interaction and is then followed by self-focusing and envelope self-modulation.

© 2000 American Institute of Physics. [S1070-664X(00)00807-7]

## I. INTRODUCTION

The interaction of terawatt (TW) laser pulses over long distances with a plasma is of great interest for the fields of laser plasma acceleration,<sup>1,2</sup> x-ray lasers,<sup>3</sup> harmonic generation,<sup>4</sup> and inertial confinement fusion with the fast ignitor scheme.<sup>5</sup> For a gaussian laser pulse, diffraction commonly limits the interaction length to the Rayleigh length  $z_R = \pi w_0^2 / \lambda_0$ , where  $w_0$  is the waist and  $\lambda_0$  the wavelength of the laser. This is why guiding over several Rayleigh lengths is important for the above applications. In the case of laser plasma accelerators, an intense laser pulse propagating in an underdense plasma can excite strong relativistic plasma waves via the ponderomotive force in the case of the laser wake field accelerator<sup>6,7</sup> (LWA). For the self-modulated LWA, the self-modulated laser wake field instability (SMLWF)<sup>8-10</sup> causes the modulation of the laser pulse envelope at the plasma frequency. Then, the ponderomotive force associated to the modulated envelope can drive a strong plasma wave. The maximum energy that electrons can gain from the relativistic plasma waves (RPW) is proportional to the product of the RPW amplitude and the dephasing length (the length over which electrons stay in an accelerating arch of the relativistic plasma waves). In order to extract maximum energy from the waves, the electrons must travel in a long and intense RPW. Previous experiments showed that the creation of such a long and intense wave can be achieved through self-focusing<sup>11,12</sup> when the laser pulse power  $P_L$  is

greater than the critical power for relativistic self-focusing  $P_C$ , where  $P_C(\text{GW}) = 17(\omega_0/\omega_p)^2$ , for a gaussian laser pulse and  $\omega_p = (n_e e^2 / \epsilon_0 m_e)^{1/2}$  is the plasma frequency. In future experiments, lower density plasmas will tend to be used in order to increase the dephasing length and the extractable energy. Current laser technology hardly provides enough power for self-focusing at lower density (at  $n_e = 10^{18}$  cm<sup>-3</sup>,  $P_C \approx 20$  TW), thus guiding the pulse in a guiding structure becomes necessary. Experiments<sup>11,13,14</sup> proved the feasibility of guiding a pulse in a preformed plasma channel over 1 cm at intensities of  $5 \times 10^{15}$  W/cm<sup>2</sup>, and more recently,<sup>15</sup> over 1 mm up to intensities of  $3 \times 10^{17}$  W/cm<sup>2</sup>. However, the interaction of a pulse with a preformed and well-characterized plasma channel was never really examined. In this paper, we studied the propagation of a pulse with intensities from  $10^{17}$  W/cm<sup>2</sup> to a few  $10^{18}$  W/cm<sup>2</sup> in a well-defined plasma channel. We observed a change in the regime of propagation and interaction when  $P_L$  becomes greater than  $P_C$ .

While self-modulated LWA experiments have always been performed in gas,<sup>16-18</sup> theory predicts that the best way to produce well-suited plasma waves for particle acceleration is through self-focusing in a preformed uniform plasma. Indeed, this scheme is ionization free; it prevents refraction induced by ionization<sup>19,20</sup> as well as blueshifting of the main radiation or any ionization instabilities.<sup>21</sup> This is another reason why the interaction of a very intense laser pulse (with  $P_L > P_C$ ) with a preformed plasma is interesting to study.

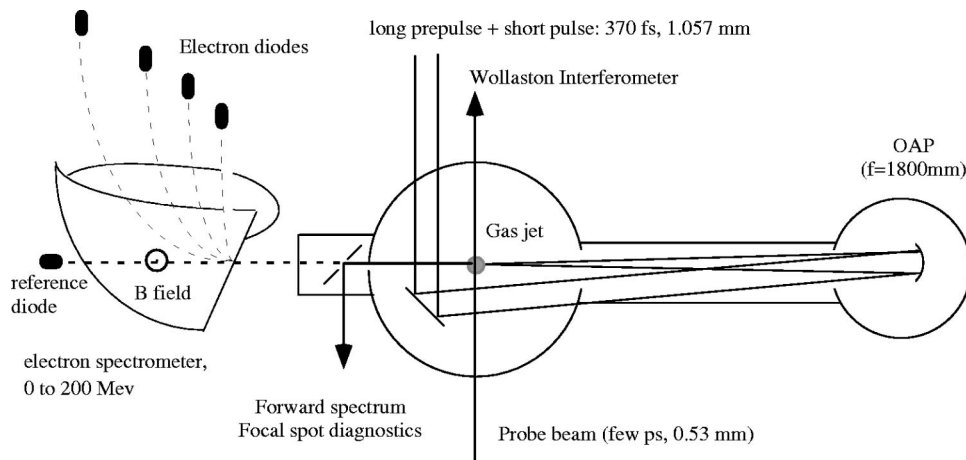


FIG. 1. Experimental setup.

Finally, our study is also of interest for the “fast ignitor” fusion concept. In this scheme, a short, intense laser pulse has to be delivered to the (imploded) dense laser-fusion capsule. The intense pulse must propagate through a long (few millimeters) region of underdense plasma and this propagation may be disturbed by forward Raman scattering (FRS) or other instabilities.

The paper is structured as follows: Sec. II first describes our experimental setup and results while Sec. III proposes interpretations of the experimental results using numerical simulations.

## II. EXPERIMENT

### A. Setup and diagnostics

The experiment was performed at Laboratoire pour l’Utilisation des Lasers Intenses (LULI) using the terawatt chirped pulse amplification (CPA) laser. The setup of the experiment is shown in Fig. 1: the 90 mm diameter terawatt (TW) laser beam was focused by a  $f/22$  off-axis parabola into a gas jet. The laser was operating at 1.057 nm providing up to 15 J on target and a duration of 370 fs at full width half maximum (FWHM). The focal spot [shown in Fig. 2(a)] was imaged using a  $f/5$  optics, giving a magnification of 12 and a spatial resolution of  $5 \mu\text{m}$ . As shown on Fig. 2(b), the radius at  $1/e^2$  in intensity is  $20 \mu\text{m}$  while the radius containing 80% of the energy is about  $35 \mu\text{m}$ . Hence powers up to 20 TW and intensities up to  $4 \times 10^{18} \text{ W/cm}^2$  could be reached, per-

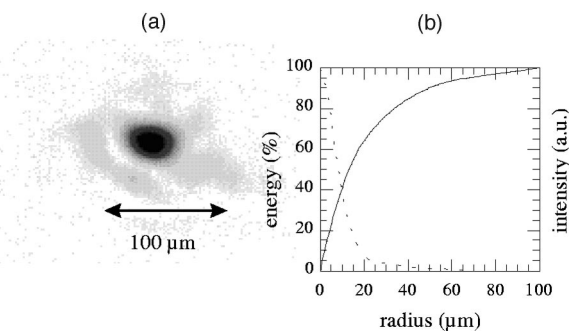


FIG. 2. (a) Image of the focal spot; (b) line out of the focal spot (dashed line); energy contained in a circle of radius  $r$  (solid line).

mitting relativistic interactions and large values of the normalized potential vector:  $a_0 = 1.8$ . The amplified spontaneous emission (ASE) of the laser chain was used as a prepulse (a few nanoseconds long) for the creation of the plasma. Its intensity (estimated to be about  $10^{14} \text{ W/cm}^2$ ) was high enough to fully ionize helium and to create a channel over the whole length of the jet. The first electrons were created by multiphoton ionization and were then heated by inverse Bremsstrahlung, creating more electrons by avalanche ionization. The plasma channel was formed by hydrodynamic expansion of the heated plasma.<sup>22,23</sup> We point out here the fact that the TW laser beam is perfectly aligned along the channel axis, because the creation beam is the ASE of the laser and it has the exact same mode and goes through the exact same path as the interaction TW beam.

To avoid refraction induced by ionization processes, as well as any kind of effects linked to the presence of a density gradient along the propagation axis, the laser beam was focused onto the sharp edge of a 4 mm diameter laminar plume of helium gas from a pulsed, supersonic gas jet located 2 mm below the focal region. The electron density out of the gas jet was controlled by changing the backing pressure. The neutral density profile [shown on Fig. 3(a)] was characterized before the experiment.<sup>24</sup> Shorter gas jets were also used in order to reach higher electron densities.

In order to obtain interferograms of the plasma, a picosecond collimated frequency doubled ( $\lambda_s = 528 \text{ nm}$ ) pulse, propagating perpendicularly to the main beam, was sent into a Wollaston interferometer. A typical interferogram of the plasma created by ASE can be found in Fig. 3(b); it was taken 2 ps before the main pulse. The laser propagates from the right to the left; the plasma is 4 mm long and about  $300 \mu\text{m}$  wide. The interferometer gave two identical images of the plasma. We kept them for clarity in the images which are presented later. The fringes are well defined and assuming cylindrical symmetry, one can retrieve the electron density distribution by Abel inverting the phase along the fringes [see Fig. 3(c)]. According to similar channel creation experiments,<sup>22</sup> the plasma temperature is usually less than 300 eV. Hence the state of the plasma is known before the interaction.

The transmitted light was reflected by a silicate plate

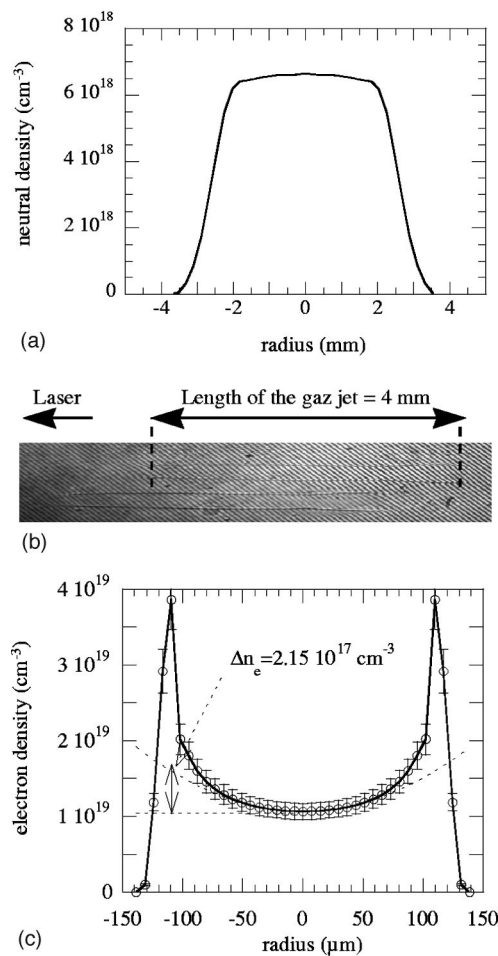


FIG. 3. (a) Neutral density profile from the 4 mm gas jet. (b) Interferogram of the plasma created by ASE and taken 2 ps before the short pulse and  $E = 10$  J. The Wollaston gave two images of the plasma, we kept them for clarity. (c) Density profile retrieved from an interferogram (circles), choosing a fringe in the middle of the channel. Parabolic fit of the profile around the axis (dotted line).

with a surface figure of  $\lambda/10$ . The entrance of the plasma was imaged with a  $f/5$  optics onto the entrance of an imaging spectrometer (100 lines/mm). The spectrum was measured using a 16 bits charge coupled device (CCD) camera. The spectral response of the imaging system and spectrometer was obtained by placing a bright blackbody source at the focal position. Deconvolved spectra could then be analyzed. The measured spectra give crucial information about the nature of the laser plasma interaction. In the experiment described in this paper, the RPW are excited by an intense pulse via the SML WF instability. In this regime the strong electromagnetic pump wave ( $\omega_0$ ,  $k_0$ ) interacts with a plasma wave ( $\omega_p$ ,  $k_p$ ) which results in two forward propagating electromagnetic waves at the Stokes ( $\omega_0 - \omega_p$ ) and anti-Stokes ( $\omega_0 + \omega_p$ ) frequencies.<sup>8-10</sup> The electromagnetic beating of these high frequency electromagnetic waves produces a low frequency modulation at  $\omega_p$ , reinforcing the original noise-level plasma wave which then scatters more sidebands, producing the growth of the instability.<sup>16</sup> Hence, from a more experimental point of view, the frequency shift of the anti-Stokes sidebands makes it possible to retrieve the electron density on axis. The same  $f/5$  lens was used to image

the entrance plane of the plasma onto a CCD camera.

Finally, an imaging electron spectrometer was set up in the forward direction in order to measure the energy of electrons produced during the interaction. A hole in the reflective optics allowed the electrons to exit the vacuum chamber through a thin 300  $\mu\text{m}$  mylar film. The electron spectrometer consisted of an electromagnet and five silicon diodes. The energy range of that spectrometer was adjustable from 0 to 200 MeV. Propagation was studied from interferograms and side images of the plasma whereas interaction was investigated using the forward spectra (electron spectra and laser spectra).

## B. Experimental results

In Fig. 3(b), one can see a typical interferogram (for a backing pressure of 60 bars) of the state of the plasma 2 ps before the arrival of the main pulse. The profile retrieved on Fig. 3(c) shows that a channel has been created by the nanosecond prepulse. The density on axis is  $1 \times 10^{19} \text{ cm}^{-3}$  and it is 4 times larger at about 100  $\mu\text{m}$  off axis. Although the density profile is not parabolic for the whole width of the channel, it is nearly parabolic over a radius of 75  $\mu\text{m}$ . A fit of the density profile for  $r < 75 \mu\text{m}$  using a function of the type  $n = n_e + \Delta n_e (r/w_0)^2$  gives a value for  $\Delta n_e$  of about  $2.1 \times 10^{17} \text{ cm}^{-3}$  (this is for  $w_0 = 20 \mu\text{m}$ ). We recall that the condition for guiding a gaussian pulse with a spot size  $w_0$  in a parabolic plasma channel such as  $n(r) = n_e + \Delta n_e (r/w_0)^2$  is  $\Delta n_e = 1/(\pi r_e w_0^2)$ . Where  $n_e$  is the electron density and  $r_e = e^2/m_e c^2$  is the classical electron radius. The theoretical value for guiding a perfect gaussian laser with a 20  $\mu\text{m}$  (and  $P_L \ll P_C$ ) radius is  $2.8 \times 10^{17} \text{ cm}^{-3}$ . The experimental value being close to the theoretical one, the plasma channel is suitable for guiding the main (TW) pulse.

For the shots which are described in what follows, the pulse energy has been kept the same so that the level of ASE would not vary from shot to shot. The repeatability of the channel formation was insured this way. On the other hand, different regimes of interaction were explored by varying the TW pulse duration. This allowed us to have shots with intensities from  $2 \times 10^{17} \text{ W/cm}^2$  to  $4 \times 10^{18} \text{ W/cm}^2$ .

### 1. Propagation at $P_L < P_C$

We consider now the case of a low power pulse propagating in the plasma channel. The pulse duration was about 7 ps, the peak intensity  $I_0 = 2 \times 10^{17} \text{ W/cm}^2$  and  $P_L < P_C$  ( $P_L/P_C = 0.8$ ). An interferogram of the plasma is shown on Fig. 4(a); it was taken about 20 picoseconds after the propagation of the laser pulse in the channel. One can see that the pulse propagated along the whole length of the jet (4 mm), leaving a density depression behind it: electrons and/or ions were radially expelled by the ponderomotive force of the laser. One can witness this in Fig. 4(a): the fringe shift at the center of the channel is significant of the density depression. The radial size of the density depression is constant all along the jet and is about 50  $\mu\text{m}$  wide (which is the resolution of the imaging). This result indicates the presence of guiding because if the pulse was not guided, its transverse dimension at the end of the jet would be about 200  $\mu\text{m}$ , and the diameter of the depression would then grow wider along the

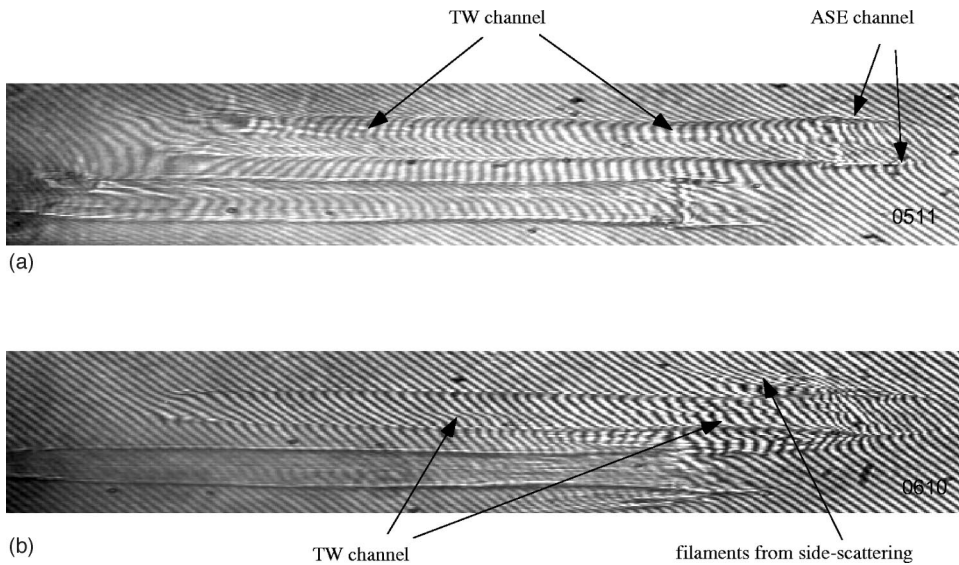


FIG. 4. (a) Interferogram of the plasma taken 20 ps after the entrance of the main pulse in the plasma. Parameters were:  $n_e=1 \times 10^{19} \text{ cm}^{-3}$ ,  $P_L/P_C=0.8$ ,  $\tau=7 \text{ ps}$ . (b) Same but with a delay of 10 ps and for the following parameters:  $n_e=1 \times 10^{19} \text{ cm}^{-3}$ ,  $P_L/P_C=17$ ,  $\tau=370 \text{ fs}$ .

propagation. This is not what we observe. In Fig. 5(a), one can see light being scattered along a 4 mm long filament. Finally, another proof of guiding can be found in Fig. 6. Figure 6(a) is a picture of the focal spot (image of the plane corresponding to the entrance of the plasma) when the laser propagates in vacuum. Figure 6(b) is an image of the entrance of the plasma. One can see that the mode of the laser has not been destroyed and the spot diameter is  $100 \mu\text{m}$ . This is due to the defocusing caused by the presence of the channel. One can calculate that a 4 mm channel guiding a gaussian pulse causes a defocusing in the image plane corresponding to a spot size of  $125 \mu\text{m}$  which is close to the measured value. In conclusion, the pulse seems to be guided by the channel over approximately  $3z_R$  (4 mm).

The spectrum of the TW pulse after interaction with the plasma is shown on Fig. 7(a). The anti-Stokes satellites are a signature of the presence of a strong plasma wave (the Stokes satellites are not visible because the sensitivity of the CCD camera is too weak for their spectral range). From the

position of the satellites, we found an electron density of  $1.1 \times 10^{19} \text{ cm}^{-3}$  which is in good agreement with the density on axis retrieved from the interferograms. It is also possible to estimate the RPW amplitude if one assumes that the ratio of the Raman satellite amplitudes is proportional to the harmonic content of the nonlinear plasma wave. The amplitude of the harmonic  $\delta n_m$  of the plasma wave as a function of the plasma wave amplitude  $\delta n_1/n_e$  is given by<sup>25,26</sup>

$$\frac{\delta n_m}{n_0} = \frac{m^m}{2^{m-1} m!} \left( \frac{\delta n_1}{n_0} \right)^m,$$

where  $m$  is the number of the harmonic. Hence the intensity ratio between the second and first harmonic is simply the

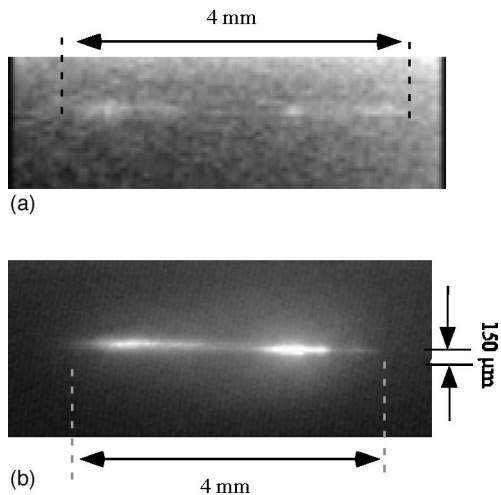


FIG. 5. Image of the scattered light from the plasma taken at  $90^\circ$  of the laser propagation axis. The image resolution is  $100 \mu\text{m}$ . (a)  $n_e=1 \times 10^{19} \text{ cm}^{-3}$ ,  $P_L/P_C=0.8$ ,  $\tau=7 \text{ ps}$ . (b)  $n_e=1 \times 10^{19} \text{ cm}^{-3}$ ,  $P_L/P_C=17$ ,  $\tau=370 \text{ fs}$ .

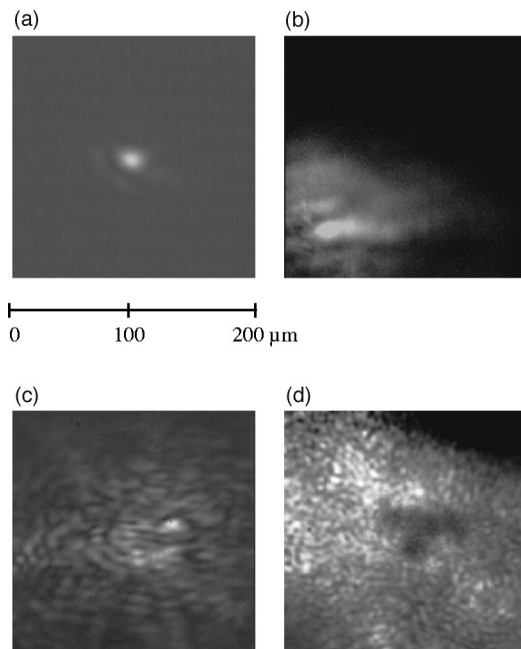


FIG. 6. Images of the entrance of the plasma ( $n_e=1 \times 10^{19} \text{ cm}^{-3}$ ). (a) Propagation in vacuum; (b) defocusing due to guiding by the channel ( $P_L/P_C=0.6$ ,  $\tau=5 \text{ ps}$ ); (c) beam break-up ( $P_L/P_C=1.5$ ,  $\tau=3 \text{ ps}$ ); (d) beam break-up ( $P_L/P_C=12$ ,  $\tau=370 \text{ fs}$ ).

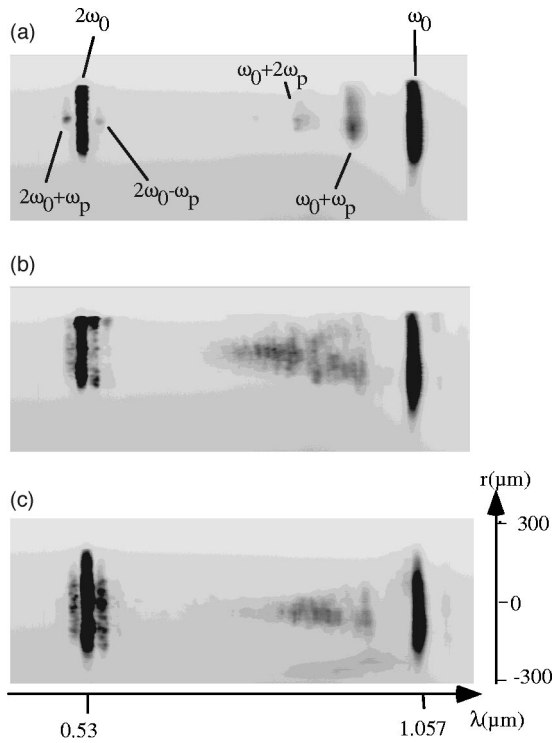


FIG. 7. Transmitted spectra. The density is always  $n_e = 1 \times 10^{19} \text{ cm}^{-3}$ , it is retrieved from (a) and from the satellites at  $2\omega_0 \pm \omega_p$  on all the pictures. (a)  $P_L/P_C = 0.8$ ,  $\tau = 7$  ps; (b)  $P_L/P_C = 2.2$ ,  $\tau = 3$  ps; (c)  $P_L/P_C = 15$ ,  $\tau = 370$  fs.

square of the plasma wave amplitude. It gives a plasma wave with an amplitude of 6%. This case is explained by the weakly relativistic linear theory of the SML WF instability, since here  $a_0 = 0.38 < 1$  and  $\delta n/n_e = 6 \times 10^{-2} < 1$ . We can consider to be in the linear part of the instability and this explains why the satellites are relatively narrow: the instability drives a plasma wave with a well-defined frequency since the growth rate is low compared to  $\omega_p$  at such intensities. If one considers that the SML WF instability is purely bidimensional,<sup>9,27,28</sup> then the laser pulse becomes modulated because it is periodically diffracted and focused by the plasma wave. In this case, assuming  $a_0 < 1$  and  $\delta n/n < 1$ , the plasma wave grows as<sup>28</sup>

$$\frac{\delta n}{n}(t, \xi) = \exp \left[ \frac{3\sqrt{3}}{4} \left( \frac{k_p^3 \omega_0^2 a_0^2}{2t_R^2} t^2 |\xi| \right)^{1/3} \right],$$

where  $\xi = z - v_g t$ ,  $k_p = \omega_p/c$ ,  $t_R = z_R/c$ .

By fitting an experimental gaussian pulse, Decker was able to calculate numerically<sup>29</sup> the initial noise due to the longitudinal ponderomotive force. An approximate estimation is

$$\left. \frac{\delta n}{ne} \right|_0 = 0.9 \pi \frac{a_0^2}{(k_p \tau c)^{2.8}},$$

where  $\tau$  is the pulse duration.

This would give a plasma wave with an amplitude of 10% after a propagation in the plasma of about 1 mm. However the growth rate given above greatly overestimates the growth of the instability because it assumes a pump which is constant in time whereas in our experiment the pump was gauss-

ian. We note that for this particular shot, no electrons were observed on the electron spectrometer since the plasma wave was far from wave breaking.

## 2. Propagation at $P_L > P_C$

For shots at  $P_L > P_C$ , the nature of the propagation is quite different. Figure 4(b) shows an interferogram taken 10 ps after the entrance of the pulse in the plasma. The pulse had the following parameters:  $P_L/P_C = 15$ ,  $\tau = 370$  fs;  $I_0 = 4 \times 10^{18} \text{ W/cm}^2$ , and the backing pressure of the jet was 60 bars. At the beginning of the channel one can see density perturbations outside of the initial plasma. They stretch over a distance of about 1 mm and make a specific angle with the propagation axis which can vary between 5 and 10 degrees. These features in the density profile indicate the presence of filaments which are scattered at the beginning of the interaction. Strong relativistic self-focusing and large angle side-scattering could explain this phenomenon. Further analysis will be given in the next section. Another filament propagates along the center of the plasma over a distance of 3 mm. The timing of the probe beam was too short (in 10 ps, light travels 3 mm) to measure the propagation of this filament to the end of the jet. However, this self-focused beamlet is guided all along the plasma. The picture on Fig. 5(b) confirms this statement: it shows a side image of the plasma. A thin filament of scattered light was present all along the jet. However, the transverse structure of the filament was not resolved by our imaging system: the resolution was about  $100 \mu\text{m}$ .

At high power, the pulse undergoes strong instabilities. This can be seen on Fig. 6, which shows images of the entrance of the jet. Figure 6(b) is the low power case, Figs. 6(c) and 6(d) correspond, respectively, to the cases  $P_L/P_C = 0.6$ ,  $P_L/P_C = 1.5$  and  $P_L/P_C = 12$ . While in the low power case, the mode is conserved, one can see that for higher powers, small structures appear. These have the size of the imaging resolution ( $5 \mu\text{m}$ ), appear when  $P_L/P_C > 1$  and their number increases with the power of the laser pulse. We think they are significant of beam break-up. The spectra shown in Fig. 7 also contain interesting features: as soon as  $P_L/P_C > 1$ , the satellites become very broad and tend to merge into each other. In Fig. 7(c), one can see a very broad satellite at  $300 \mu\text{m}$  off axis; it is in correlation with the observation of the filaments propagating outside of the plasma cylinder on Fig. 4(b). It is important to note that on these shots, no intense electron signal was detected on the electron spectrometer. In similar experiments, the broadening of the Raman satellites has been identified as a characteristic of wave breaking. However in our experiment, this interpretation does not apply because longitudinal relativistic wave breaking did not occur for those shots.

Finally we used a shorter gas jet to reach higher densities (the density for these shots was  $2 \times 10^{19} \text{ cm}^{-3}$ ). Except for the fact that the propagation distance is shorter, the interaction was of the same nature as seen in Fig. 8. For  $P_L < P_C$  we have well-defined satellites on the spectrum. For  $P_L = 28P_C$ , the spectrum on Fig. 8(a) indicates a type of interaction similar to the cases studied previously. The interfero-

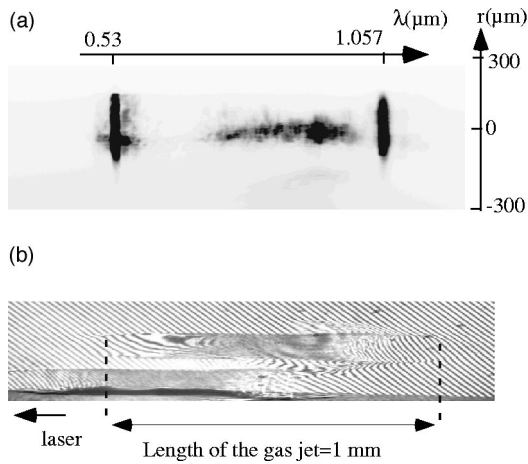


FIG. 8. Interaction with a 1 mm gas jet.  $n_e = 2 \times 10^{19} \text{ cm}^{-3}$ ,  $P_L/P_C = 28$ ,  $\tau = 370 \text{ fs}$ . (a) spectrum of the transmitted light. (b) interferogram of the plasma 10 ps after the main pulse.

gram on Fig. 8(b) also indicates the presence of density perturbation at large angles at the entrance of the plasma. The fringes are not well defined here because the plasma was expanding too fast. For this case, a lot of MeV electrons were detected. The electron distribution was a decreasing function of the energy and electrons with energies up to 60 MeV were detected. A typical electron spectrum is presented in Fig. 9.

In this high power regime, the interaction was highly nonlinear and dominated by strong instabilities. This regime cannot be modeled using simple weakly relativistic nonlinear models and numerical simulations are necessary.

To summarize our experimental results: for a long propagation (4 mm) at low power ( $P_L/P_C = 0.8$ ), we observed guiding of the laser pulse over 4 mm ( $3z_R$ ). We also observed the generation of a plasma wave with an amplitude of 6%, but no electrons were produced. For a long propagation at high power ( $P_L/P_C > 1$  and up to 12), we observed beam break-up of the pulse and an interaction dominated by instabilities. No relativistic electrons ( $> 1 \text{ MeV}$ ) were detected. For a short propagation at high power and higher density ( $2 \times 10^{19} \text{ cm}^{-3}$  and  $P_L/P_C = 28$ ), the same propaga-

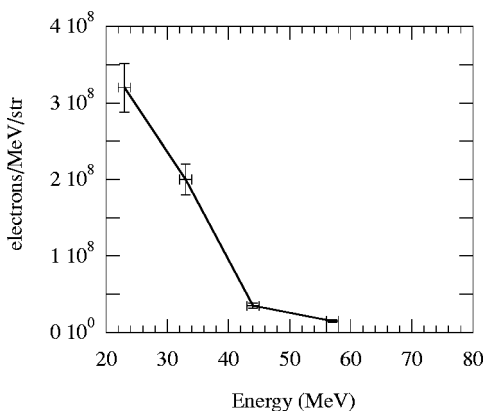


FIG. 9. Electron spectrum for the shot of Fig. 8.

tion and interaction as the previous case were observed. The generation of relativistic electrons was also observed.

### III. NUMERICAL SIMULATIONS AND INTERPRETATIONS

#### A. Numerical simulations

The simulations have been done using the code WAKE<sup>30</sup> in its slab geometry. This code is based on the fast time averaging of the equations for the motion of particles and for the generation of electromagnetic wake fields. It offers an alternative to particle-in-cell (PIC) codes for propagations over long distances. Nevertheless, the model it uses contains approximations, and not all the physics of the interaction is described. It is valid only for tenuous plasma with  $\omega_p \ll \omega_0$ . It does not describe the generation of hot electrons; only electrons for which  $(1 - v_z/c) \gg \omega_p/\omega_0$  are taken into account. Backscattering instabilities are not considered because the radiation is assumed to be mainly forward propagating. Finally, the code cannot predict the generation of harmonics because it does not resolve the laser frequency (some equations are fast time averaged).

We used the code in order to simulate the propagation over 4 mm of a short pulse with  $P_L/P_C \sim 10$  in a preformed plasma channel. The parameters of the simulation were the following:  $\lambda_0 = 1.057 \mu\text{m}$ ,  $w_0 = 23.8 \mu\text{m}$  ( $z_R = 1.68 \text{ mm}$ ),  $\tau_{\text{FWHM}} = 300 \text{ fs}$ ,  $P_L/P_C = 6.3$ ,  $I_0 = 1.2 \times 10^{18} \text{ W/cm}^2$ . The density distribution of the plasma was the measured density profile. The size of the simulation box was  $120k_p^{-1} \times 2z_R$ . The validity of the code at such powers was also tested by comparing its results to the result of a PIC simulation for the first 500  $\mu\text{m}$  of propagation. After a propagation of 500  $\mu\text{m}$ , both simulations show strong side scattering; there is a very good qualitative agreement between the two codes. The numerical values are slightly different because the noise which triggers the instability can have different causes in the two codes.

Figure 10 presents the results of the full simulation. Each picture represents the intensity distribution in the pulse reference frame for a given  $z$  of the propagation and as a function of time. At the beginning of the interaction, the back of the laser pulse undergoes a very strong side scattering at large angles (see first picture in Fig. 10). Then the front and middle part of the pulse self-focus and the self-modulation instability begins to grow affecting mainly the front and middle part of the pulse (second picture). The instability continues to grow during the propagation of the laser pulse along the plasma. A lot of laser energy goes off to the sides and is not trapped in the plasma channel whereas a strongly self-modulated structure seems to propagate on axis (third picture). The same images on a logarithmic scale show that the plasma channel is inefficient for trapping the large angle side scattering generated at the beginning of the plasma. On the other hand, scattered light created later stays confined within the channel. One can also see that the plasma channel guides without deterioration the very front of the pulse for which  $P_L/P_C < 1$ . The same simulation was also run for a uniform plasma. The nature of the interaction was very much the same except for these minor details, showing that the

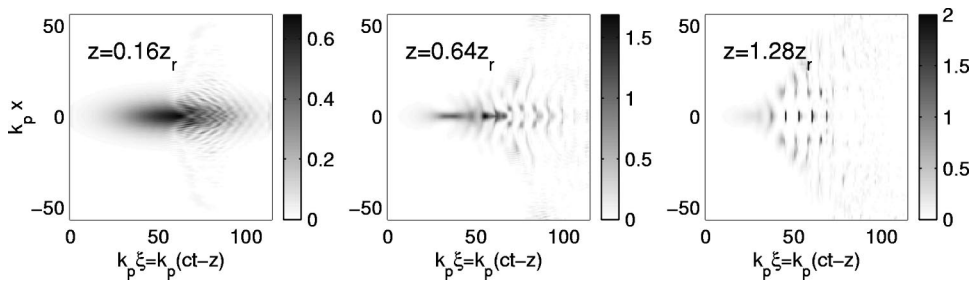


FIG. 10. Simulated propagation of the pulse. The pulse parameters are  $P_L/P_C=6.7$ ,  $\tau=300$  fs,  $w_0=23.8 \mu\text{m}$  (Gaussian pulse). The simulation includes a fit of the experimental plasma channel.

plasma channel plays a minor role in the interaction at such powers. Figure 11 shows the simulated spectra of the transmitted light at the output of the plasma (after a propagation of 4 mm). The satellites are very broad and can hardly be distinguished and there is a rather strong spectral signal off axis.

We note that the simulation might have underestimated certain effects such as self-focusing and ponderomotive blow out for different reasons. First, the slab geometry of the simulation tends to underestimate these effects and second the intensity chosen for the simulation is smaller than the intensity of the experimental case presented in Fig. 7(c).

**B. Interpretation and discussion**

One can see a very good agreement between experiment and theory: there is strong Raman side scattering at the beginning of the interaction; it is then followed by strong self-focusing and SML WF. On the spectrum, we obtained similar spectral structure with no distinct satellites.

The fact that strong scattering at large angles is present at the beginning of the interaction can be easily understood: scattering at large angles is mainly a three wave process. The plasma waves are resonantly driven by the beat wave pattern of the main radiation at  $\omega_0$  and the Stokes wave at  $\omega_0 - \omega_p$ . As explained earlier (see Sec. II), the SML WF instability is a four wave process. In this case, the beatings of the main radiation and the satellite waves largely cancel out.<sup>31</sup> The consequence is that the growth rate of the large angle scattering instability is larger, which is why it grows before the SML WF. Another important point is that the number of exponentiations  $N_{e\text{-folding}}$  of the large angle instability de-

pends on the focal spot size<sup>32</sup> as long as the scattering angle  $\theta$  (see Fig. 12 for a schematic) satisfies  $\theta < \theta_C$ ; where  $\theta_C = 2 \arctan(c\tau/2w_0)$  is a critical angle. In the Raman (Compton) regime,  $N_{e\text{-folding}}$  scales as  $w_0^{1/2}(w_0^{1/3})$ . Hence, the fact that the pulse width is large (compared to other experiments) is also in favor of large angle side scattering. The reason for a precise angle of scattering is unclear: theory<sup>32</sup> says that the growth rate is larger for larger angles up to the critical angle  $\theta_C$  ( $=140^\circ$  for our experiment), but the instability needs a noise to start on and this noise can be provided through several mechanisms. The final scattering angle  $\theta$  will maximize the product  $\exp[N_{e\text{-folding}}(\theta)] \times \delta E_{\text{noise}}(\theta)$ , where  $N_{e\text{-folding}}$  is the number of exponentiation of the large angle instability and  $\delta E_{\text{noise}}$  an electromagnetic noise at frequency  $\omega_0 - \omega_p$ . This noise can come from the initial scattering of the laser on thermal density fluctuations in the plasma or also from scattering on the wake field created by the ponderomotive force of the laser. The wake field generated by a laser is

$$\frac{\delta n(r)}{n} = \omega_p^{-1} \int_0^t dt' \sin \omega_p(t-t') c^2 \nabla^2 \frac{a^2}{2} \propto \nabla^2 \frac{a(r)^2}{2}.$$

By simply Fourier transforming this expression, one can find the spectrum for the initial plasma waves:  $\delta n(k_\perp)/n \propto \delta E_{\text{noise}}(k_\perp)$ . Electromagnetic waves ( $\mathbf{k}_s, \omega_s$ ) can scatter at an angle  $\theta$  on these plasma waves and  $k_s$  verifies:  $\sin(\theta) = k_\perp/k_s$ . Thus, it is possible to obtain  $\delta E_{\text{noise}}(\theta)$  this way. Calculating  $\exp[N_{e\text{-folding}}(\theta)] \times \delta E_{\text{noise}}(\theta)$ , one finds that the instability should develop at an angle which varies from  $2^\circ$  to  $6^\circ$  with a maximum at  $4^\circ$  which is close to the experimental value. These simple considerations give an insight on the reason why the side Raman instability develops at a specific angle. In any case, as seen on the interferogram Fig. 4(b), beamlets of scattered light at  $\omega_s = \omega_0 - \omega_p$  leave the plasma cylinder and ionize the surrounding gas. Ionization could cause a strong blue-shifting of these radiation, explaining the very broad continuous feature off axis on Fig. 7(c).

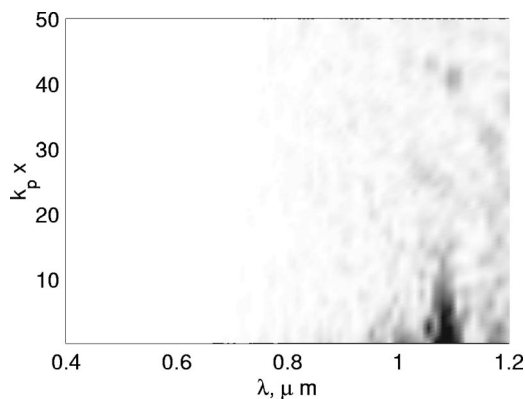


FIG. 11. Simulated spectrum of the transmitted light. Same parameters as Fig. 10.

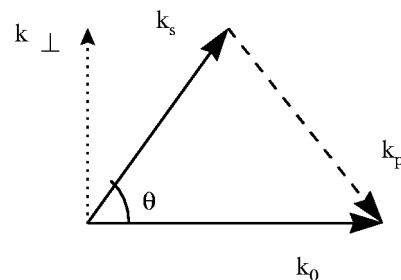


FIG. 12. Geometry of Raman side scattering.

In the high power case, the main difference on the forward spectra appears in the broadening of the Raman satellites. This is not surprising if one considers that the temporal envelope of the plasma wave is an increasing exponential function (at least at the beginning of the instability)  $\exp(\gamma t)$ , where  $\gamma$  is the growth rate of the instability. The spectrum of such a wave has a width which is proportional to  $\gamma$ . Furthermore,  $\gamma$  scales as  $\sqrt{I}$  in the weakly relativistic limit. Hence for the low power case, the laser intensity is low and  $\gamma/\omega_p = 0.02 \ll 1$ . This gives a narrow spectral peak at  $\omega_p$  on the spectrum. This is what we observe in Fig. 7(a): there is a narrow satellite at  $\omega_0 + \omega_p$ , significant of the coupling between the laser and the plasma. In the high power case, the intensity is larger; so is  $\gamma/\omega_p$  ( $\approx 0.1$ ), making the spectral peak wider. Physically, one can understand that when the growth rate becomes comparable to  $\omega_p$ , the plasma wave can oscillate at nonresonant frequencies. There are other arguments to explain the broadening of the satellites. First, as shown in the simulation, after self-focusing of the beam, the self-modulation instability takes place on axis but there is still a major amount of light which is scattered off axis and trapped in the channel. In the channel, the scattered light interacts with electron densities stretching over a range from  $1 \times 10^{19} \text{ cm}^{-3}$  to  $4 \times 10^{19} \text{ cm}^{-3}$ . This contributes largely to the broadening of the satellites. Finally, the strong transverse ponderomotive force generates density gradients in the vicinity of the propagation axis. This has similar effects and contributes to the broadening of the spectral features.

#### IV. CONCLUSION

We have investigated experimentally the interaction of an ultraintense laser pulse with a preformed plasma channel. In the long pulse case, i.e., for powers smaller than the critical power for self-focusing, the pulse was guided in the channel over 4 mm ( $3z_R$ ). A resonant plasma wave ( $\delta n/n = 6\%$ ) was excited through the SML WF instability. The plasma wave was far from breaking and no hot electrons (with energies larger than 1 MeV) were generated. In the high power case, a very nonlinear interaction was taking place. Using numerical simulations, we were able to analyze the dynamics of the interaction. First, filaments propagating at  $5^\circ$  to  $10^\circ$  to the axis were created through intense side scattering; the filaments then ionized the gas outside of the plasma and were not trapped in the channel. Then self-focusing and self-modulation of the pulse occurred but no very intense resonant plasma waves were generated. The generation of a large number of MeV electrons occurred for a density of  $2 \times 10^{19} \text{ cm}^{-3}$  ( $P_L/P_C = 28$ ).

#### ACKNOWLEDGMENTS

This experiment was done under European TMR Contract No. ERBFMGECT950044. The experiment was supported by grants from the EPSRC, the Human Capital and

Mobility Program of the European Community. The work of A. Solodov was supported in part by the Russian Foundation for Basic Research (Grants Nos. 98-02-17205 and 99-02-16399).

- <sup>1</sup>T. Tajima and J. Dawson, Phys. Rev. Lett. **43**, 267 (1979).
- <sup>2</sup>E. Esarey, P. Sprangle, J. Krall, and A. Ting, IEEE Trans. Plasma Sci. **24**, 252 (1996).
- <sup>3</sup>N. H. Burnett and G. D. Enright, IEEE J. Quantum Electron. **26**, 1797 (1990).
- <sup>4</sup>X. F. Li, A. L'Huillier, M. Ferray, L. A. Lompre, and G. Mainfray, Phys. Rev. A **39**, 5751 (1989).
- <sup>5</sup>M. Tabak, J. Hammer, M. E. Glinsky, W. L. Kruer, S. C. Wilks, J. Woodworth, E. M. Campbell, M. D. Perry, and R. J. Mason, Phys. Plasmas **1**, 1626 (1994).
- <sup>6</sup>L. M. Gorbunov and V. I. Kirsanov, Sov. Phys. JETP **66**, 290 (1987).
- <sup>7</sup>F. Amiranoff, S. Baton, D. Bernard, B. Cros, D. Descamps, F. Dorchies, F. Jacquet, V. Malka, G. Matthieussent, J. R. Marques, P. Mine, A. Modena, P. Mora, J. Morillo, and Z. Najmudin, Phys. Rev. Lett. **81**, 995 (1998).
- <sup>8</sup>N. E. Andreev, L. M. Gorbunov, V. I. Kirsanov, A. A. Pogossova, and R. Ramazashvili, JETP Lett. **55**, 571 (1992).
- <sup>9</sup>T. M. Antonsen and P. Mora, Phys. Rev. Lett. **69**, 2204 (1992).
- <sup>10</sup>P. Sprangle, E. Esarey, J. Krall, and G. Joyce, Phys. Rev. Lett. **69**, 2200 (1992).
- <sup>11</sup>K. Krushelnick, A. Ting, C. I. Moore, H. R. Burris, E. Esarey, P. Sprangle, and M. Baine, Phys. Rev. Lett. **78**, 4047 (1997).
- <sup>12</sup>C. E. Clayton, D. Gordon, K. A. Marsh, C. Joshi, V. Malka, Z. Najmudin, A. Modena, A. E. Dangor, D. Neely, and C. Danson, Phys. Rev. Lett. **1**, 100 (1998).
- <sup>13</sup>S. P. Nikitin, T. M. Antonsen, T. R. Clark, Y. Li, and H. M. Milchberg, Opt. Lett. **22**, 1787 (1997).
- <sup>14</sup>Y. Ehrlich, C. Cohen, A. Zigler, J. Krall, P. Sprangle, and E. Esarey, Phys. Rev. Lett. **77**, 4186 (1996).
- <sup>15</sup>S.-Y. Chen, G. S. Sarkisov, A. Maksimchuk, R. Wagner, and D. Umstadter, Phys. Rev. Lett. **80**, 2610 (1998).
- <sup>16</sup>A. Modena, A. E. Dangor, Z. Najmudin, C. E. Clayton, K. Marsh, C. Joshi, V. Malka, C. B. Darrow, C. Danson, D. Neely, and F. N. Walsh, Nature (London) **377**, 606 (1995).
- <sup>17</sup>D. Umstadter, S.-Y. Chen, A. Maksimchuk, G. Mourou, and R. Wagner, Science **273**, 472 (1996).
- <sup>18</sup>C. I. Moore, A. Ting, K. Krushelnick, E. Esarey, R. F. Hubbard, B. Hafizi, H. R. Burris, C. Manka, and P. Sprangle, Phys. Rev. Lett. **79**, 3909 (1997).
- <sup>19</sup>P. Chessa, E. D. Wispelaere, F. Dorchies, V. Malka, J. R. Marques, G. Hamoniaux, P. Mora, and F. Amiranoff, Phys. Rev. Lett. **82**, 552 (1999).
- <sup>20</sup>V. Malka, E. D. Wispelaere, J. R. Marques, R. Bonadio, F. Amiranoff, F. Blasco, C. Stenz, P. Mounaix, G. Grillon, and E. Nibbering, Phys. Plasmas **3**, 1682 (1996).
- <sup>21</sup>T. M. Antonsen and Z. Bian, Phys. Rev. Lett. **82**, 3617 (1999).
- <sup>22</sup>V. Malka, E. D. Wispelaere, F. Amiranoff, S. Baton, A. Modena, R. Haroutunian, R. Bonadio, C. Coulaud, D. Puissant, C. Stenz, and S. Hüller, Phys. Rev. Lett. **16**, 2979 (1997).
- <sup>23</sup>C. G. Durfee III, J. Lynch, and H. M. Milchberg, Phys. Rev. E **51**, 2368 (1995).
- <sup>24</sup>V. Malka, C. Coulaud, J.-P. Geindre, V. Lopez, Z. Najmudin, D. Neely, and F. Amiranoff, Rev. Sci. Instrum. (in press).
- <sup>25</sup>E. A. Jackson, Phys. Fluids **3**, 831 (1960).
- <sup>26</sup>F. F. Chen, Phys. Scr. **T30**, 14 (1990).
- <sup>27</sup>E. Esarey, J. Krall, and P. Sprangle, Phys. Rev. Lett. **72**, 2887 (1994).
- <sup>28</sup>N. E. Andreev, L. M. Gorbunov, V. I. Kirsanov, A. A. Pogossova, and A. S. Sakharov, Plasma Phys. Rep. **22**, 379 (1996).
- <sup>29</sup>C. D. Decker, Ph.D. Dissertation, 1994.
- <sup>30</sup>P. Mora and T. M. Antonsen, Phys. Plasmas **4**, 217 (1997).
- <sup>31</sup>N. E. Andreev, V. I. Kirsanov, L. M. Gorbunov, and A. S. Sakharov, IEEE Trans. Plasma Sci. **24**, 363 (1996).
- <sup>32</sup>T. M. Antonsen and P. Mora, Phys. Fluids B **5**, 1440 (1993).